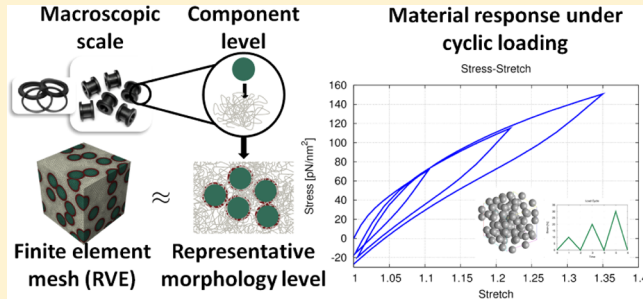


Finite Element-Based Micromechanical Modeling of Microstructure Morphology in Filler-Reinforced Elastomer

Deepanshu Sodhani* and Stefanie Reese

Institute of Applied Mechanics, RWTH Aachen University, Mies-van-der-Rohe Strasse 1, Aachen, Germany

ABSTRACT: Characteristic properties of elastomers including their fatigue behavior and wear resistance can be tailored by embedding them with filler particles. Along with enhancing the overall properties of the system, filler particles also induce some inelastic effects including the Mullins and the Payne effect. In this paper, computational modeling using finite element methods has been employed to study the mechanical behavior of such systems. A nonlinear model is applied, to predict the macroscopic large deformation behavior, with morphology evolution and deformation occurring at the microscopic level, using the representative volume element (RVE) approach. The approach is based on a micro mechanically motivated hyper-elastic constitutive model, describing the elastomeric matrix within the RVE. In order to simulate the breakdown and reaggregation of filler networks, effects like the change in the glass transition temperature in the vicinity of filler particles, are incorporated in the system. The implementation is designed to be robust, for accommodating large rotations and stretches of the matrix local to, and between, the nanoparticles. The nanocomposite microstructure is reconstructed at the RVE level using a random particle generation algorithm, with the assumption of periodicity. Computational experiments using this methodology enable prediction of the strain softening behavior of filled elastomers, observed experimentally, and to understand the behavior of the interphase between two filler particles and its effect on the characteristic material behavior of filled elastomers.



1. INTRODUCTION

Stronger, stiffer elastomeric materials are attractive to numerous industries due to their lightweight, easy manufacturing and low cost. Reinforcement of elastomer matrices with inorganic nanoparticles produces composite materials that exhibit enhanced mechanical and thermo mechanical properties without significant increase in the weight of the material. Excellent stiffness and strength are achieved while utilizing far less high-density inorganic material than is utilized in conventional composites. Independent of whether the nano filler is spherical (carbon black), cylindrical (carbon nanotubes) or a platelet (clay), the efficiency of the inorganic nano reinforcement depends on three parameters: filler mechanical properties, filler aspect ratio and adhesion between the matrix and filler. However, along with the enhancements in the mechanical properties, inelastic stress softening phenomena like the Payne effect¹ and the Mullins effect² are also encountered.

Huber and Vilgis,³ Berriot et al.,⁴ Klüppel,⁵ and Vilgis et al.⁶ provide a good overview of important physical phenomena present in filled elastomers. Several reinforcement mechanisms at different length scales are identified. One of these is due to the roughness of the filler surface which influences the adsorption behavior between filler and polymer. The surface roughness, expressed in terms of the surface fractal dimension, is closely related to surface activity and finally the energy distribution on the filler surface.^{5,7} The latter correlates with the polymer–filler interaction strength in the way that any kind of disorder or heterogeneity induces additional attractive inter-

action. Another important contribution to the reinforcement of elastomers is the so-called hydrodynamic reinforcement. The geometrically very complex structure of the filler aggregates leads to a sensitive dependence of the stiffness moduli on the branched aggregate structure.⁶ Related to that is also the strain amplification discussed, e.g., in Dupret et al.⁸

The admixture of fillers causes certain peculiar inelastic effects in the material behavior of filler-reinforced polymers. The most common are stress softening under dynamic loading (Payne effect), and under quasi-static loading (Mullins effect). A number of modeling concepts have been used to represent the physical behavior of filled elastomers but we restrict ourselves to models which at least partially incorporate the physical behavior at the micro scale, in particular for the Mullins effect. An ideal case of the Mullins effect is illustrated in Figure 1, while the real case is illustrated in Figure 2.

In their work on the Mullins effect, Govindjee and Simo¹⁰ introduce a relation for the strain amplification, i.e., a relation between averaged macroscopic and matrix material nonlinear strain measures. The free energy function splits into contributions from chains between cross-links and chains running between particles. Strain-induced matrix-particle debonding is considered only in the second part. In contrast to the latter authors Marckmann et al.¹¹ extend the eight-chains

Received: November 22, 2013

Revised: March 24, 2014

Published: April 29, 2014

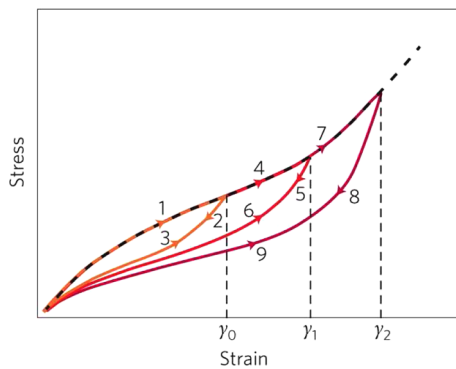


Figure 1. Illustration of the ideal Mullins effect. Softening occurs if the material is cyclically deformed, that is, during the second cycle a lower force is needed to reach the amplitude γ_0 than in the first cycle (path 3 versus path 1). If the amplitude is increased beyond γ_0 , the loading curve (path 4) follows the path of a single loading experiment (black dashed line). If the material is cyclically loaded to a new maximal amplitude (γ_1 or γ_2), again softening is observed (path 6 versus path 4, or path 9 versus path 7).⁹

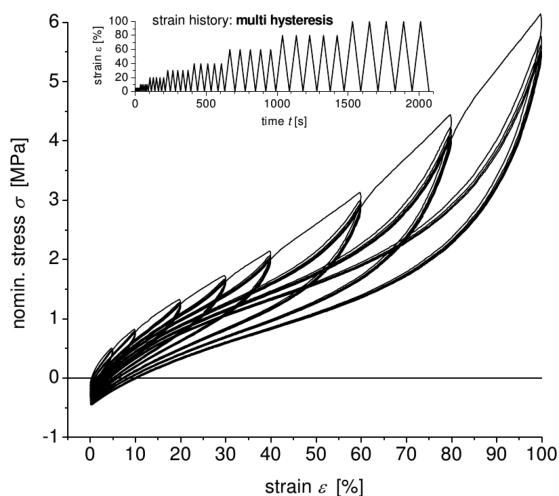


Figure 2. Real Mullins effect.¹⁸

model of Arruda and Boyce¹² in such a way that the two main constants (shear modulus and average number of links per chain) become functions of the maximum chain stretch ratio. Göktepe and Miehe¹³ include the breakdown of chain-particle bonds into their previously developed microsphere model. A common aspect of the three models is the fact that different loading rates do not lead to different results; i.e., the models are rate-independent.

Another approach (see, e.g., Klüppel⁵) is the cluster-cluster aggregation which can be mathematically described by expressing the local solid fraction as a function of the primary aggregate size, the cluster size, the solid fraction of primary aggregates and other physical quantities. In the work of Lin and Lee¹⁴ and the recent paper of Dargazany and Itskov¹⁵ the nonlinear elastic behavior of single aggregates is formulated by means of a new analytical micromechanical model based on an angular averaging approach. In recent works, Lorenz et al.¹⁶ use the concept of representative directions to effectively simulate the macroscopic response of filled elastomers based on the morphology of the microstructure. Other theories like molecules slipping, chain disentanglement, chain retraction and network rearrangement are discussed in Diani et al.¹⁷ In

summary it can be said that for the moment there does not exist an unanimously agreed upon theory to describe the Mullins effect.

To the knowledge of the authors, full-field simulation of filled elastomers accounting for the morphology of their microstructure has not been extensively studied. The work of Gusev¹⁹ and Gusev and Lurie²⁰ can be considered in this direction, where they study the viscoelastic behavior of particulate-reinforced polymers, with the emphasis on the Payne effect. The benefit of this approach over other approaches is the predictive capability of the model relating one or more microstructural effects to a macroscopic phenomenon. The main goal of the present work is to develop a micromechanically motivated finite element model of filler-reinforced elastomers which serves to better understand and qualitatively analyze their complex physical behavior. In this work, we demonstrate the effect of various filler concentrations and filler–filler interactions on the morphology of the microstructure. For this the microstructure of the filled elastomer system is schematically represented in Figure 3.

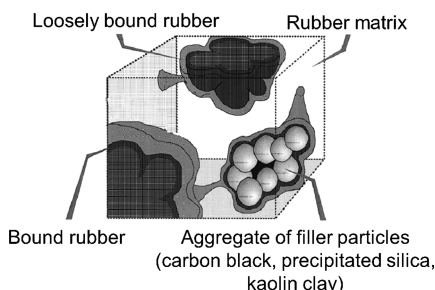


Figure 3. Schematic representation of filler-reinforced elastomers.²¹

The microstructure of the system consists of two main components, namely aggregated filler particles and elastomer chain matrix. The matrix is further divided into two phases, the so-called bound elastomer close to the surface of the filler particle which transforms into a rubbery phase away from the surface of the filler particle. To illustrate the modeling and morphology of the system under loading this paper is organized as follows. In section 2, we discuss the mechanical behavior of the single phase matrix material. In section 3, we illustrate the importance of the second phase or the so-called bound rubber. This is followed by the discussion on modeling the multiphase elastomer matrix in section 4. Micromechanical modeling of filled elastomer is elaborated in section 5. Results of numerical simulations are discussed and comments on the performance of the proposed numerical simulation method are presented in section 6. The paper closes with a summary and an outlook to future work.

2. SINGLE PHASE MATERIAL LAW FOR BULK RUBBER

To begin with, we first lay the foundation of a physically reasonable description of the mechanical behavior of the single phase rubber matrix. One fundamental material property of rubber material is its high elasticity which permits stretching of several hundred percent. The reason for this behavior is the particular micro structure of rubber which is characterized by a huge number of chain-like macromolecules forming a three-dimensional network. The material exhibits so-called statistical behavior. Considering the acceptable results and model's dependence on only two material parameters, the Arruda and

Boyce model is used to demonstrate the behavior of bulk rubber matrix. The model depends on the right Cauchy–Green tensor C . The material response has further been split into isochoric and volumetric parts

$$W_r = W_{r\text{-iso}}(\bar{C}) + W_{r\text{-vol}}(J) \quad (1)$$

where $\bar{C} = \bar{F}^T \bar{F}$ with $\bar{F} = J^{-1/3} F$ denotes the unimodular right Cauchy–Green tensor.

The Helmholtz free energy for the isochoric part of the hyperelastic response of rubber material is given by

$$W_{r\text{-iso}} = nk\theta N_0 \left[\lambda_r \mathcal{L}^{-1}(\lambda_r) + \ln \frac{\mathcal{L}^{-1}(\lambda_r)}{\sinh \mathcal{L}^{-1}(\lambda_r)} \right] \quad (2)$$

where n is the chain density, k is the Boltzmann's constant, θ is the room temperature, N_0 is the number of chain links, λ_r is the chain stretch, and $\mathcal{L}^{-1}(\cdot)$ is the inverse of the Langevin function which incorporates the locking of polymer chains at high stretches. The product of n , k , and θ constitutes the shear modulus μ_0 of rubber material.

The statistical properties of a single chain only depend on geometrical parameters and hence can be modeled in a relatively simple way. However, intermolecular interactions, in particular the effect of the well-known van der Waals forces, cannot be completely neglected because they are mainly responsible for the fact that rubber is almost incompressible. Hence, to incorporate that and give the structure additional volumetric stiffness, the addition of a penalty function such as

$$W_{r\text{-vol}} = \frac{K}{4}(J^2 - 1 - 2 \ln(J)) \quad (3)$$

where $J = \det F$ denotes the determinant of the macroscopic deformation gradient F and K is the bulk modulus, has been widely suggested in literature.

In principal various other micromechanically motivated rubber material models like the tube model of Edwards and Vilgis²² or the Böhl and Reese²³ model can also be used. After having identified the material law used to describe the bulk of the matrix, let us now focus on the formulation of bound rubber around the filler particles where the rubber matrix is considered to be in its glassy state.

3. BOUND ELASTOMER

Bound polymer is a binder layer around filler particles. The physical–chemical properties of the carbon black surface are influencing the adjacent elastomer. At a distance of 1–3 nm from the surface of particles, the polymer is in a glassy state, then the polymer chains become more active, and this layer with changed properties transfers to the loosely bound rubber. Generally, the experimental method of identifying the amount of bound rubber is as follows: an uncured sample is treated with the appropriate solvent for a sufficient time, in such a manner that all the extractable chains are dissolved. Then the extracted material is dried and the bound rubber is obtained by weighing.²¹ Apparently, the result strongly depends on the experimental conditions (temperature, time of storage of samples and time of sample holding in the solvent, etc.). The obtained mass fraction of bound polymer can be found in the literature. Although this result is definitely related to the properties of the binder and the experimental conditions, in the present investigation, only the kind of the filler and its volume fraction have been taken into consideration. For different experimental conditions, kinds, and concentrations of the filler,

the thickness changes from 4.5 to 6 nm. These values are higher than the thickness of the rigid layer (1–3 nm).

This is indicative that the undissolved binder contains not only the glassy part, but also the adjacent polymer chains, which are in another state. As explained by Berriot et al.⁴ and then extended by Merabia et al.,²⁴ there exists a hypothesis that the glassy layer transforms to a rubbery layer, and the total thickness of both layers is approximately equal to 10 nm. Bound rubber plays a crucial role in reinforcement of filled elastomer. Overlapping of bound rubber around different filler particles leads to a formation of glassy bridges which in turn leads to the formation of filler network inside the system, see Figure 4. Filler networks in turn behave as short fibers, forming

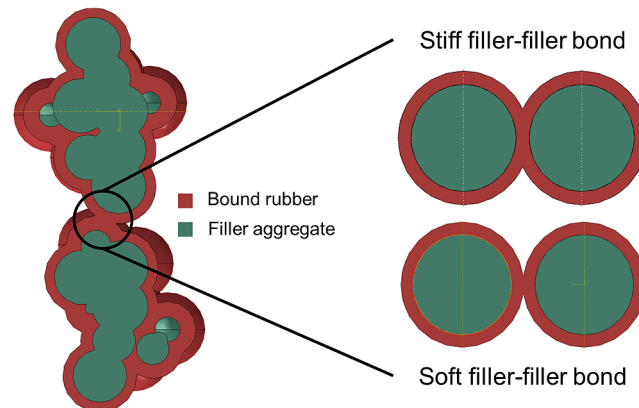


Figure 4. Filler network formation due to the overlap of bound rubber.

a path for stress flow in the system. The phenomenon of stress softening is often described as yielding and healing of these glassy bridges during loading and unloading, respectively. The healed glassy bridges are considered to have less stiffness compared to the virgin glassy bridges.⁵ The modeling of bound rubber as part of the matrix is explained in the following section.

4. MULTIPHASE MATERIAL LAW FOR BOUND RUBBER

As mentioned in the previous section, the matrix is divided into two phases. There exists a bound rubber phase close to the filler particles which transforms into a rubbery phase away from the filler particle. Let us now use the indices "r" and "b" for rubbery and bound parts of the matrix. As already mentioned the yielding and healing behavior of the bound rubber region leads to stress softening of filled elastomer composite. To incorporate that we model the bound rubber region by means of a model of finite plasticity with isotropic hardening. The total Helmholtz free energy for the matrix per unit reference volume can be represented by means of a simple rule of mixtures

$$W_{\text{matrix}} = (1 - \phi)W_r(C) + \phi W_b(C, C_p) \quad (4)$$

where ϕ denotes the fraction of bound rubber in the matrix, which is a function of distance from the surface of the filler particle. This accounts for the transition of the matrix from bound rubber to bulk rubber around the filler particles. The scalar quantity ϕ is elaborated upon in the next section. C and C_p represent the right Cauchy–Green tensor and the so-called "plastic" right Cauchy–Green tensor, respectively. Essentially the rubbery part of the matrix is much softer than the bound rubber region of the matrix. Consequently different sets of

material properties have to be chosen for the two different phases.

Finite Plasticity with Isotropic Hardening. Classical multiplicative decomposition of deformation gradient into elastic and plastic parts $F = F_e F_p$ is well established in the finite strain regime. The model described here has been proposed earlier by Reese and Wriggers²⁵ and then by Dettmer and Reese.²⁶ An improved algorithmic implementation version of this model as suggested by Vladimirov et al.^{27,28} has been used in this work. For detailed derivation please refer to the above-mentioned papers. In this case F_e is assumed to represent the deformation caused by the stretching and rotation of the bound polymer chains, whereas F_p corresponds to the plastic deformation of the glassy bridges between filler particles. Based on the principle of material objectivity, the free energy depends on the deformation only through the elastic right Cauchy–Green tensors $C_e = F_e^T F_e = F_p^{-T} C F_p^{-1}$. Here, C denotes the right Cauchy–Green tensor and $C_p = F_p^T F_p$ is the plastic right Cauchy–Green tensor. The Helmholtz free energy per unit undeformed volume decomposes additively into two parts: $W_b = W_{b-elas}(C_e) + W_{b-isot}(\kappa)$. The first part W_{b-elas} describes the elastic material properties and the second term $W_{b-isot}(\kappa)$ represents the additional amount of stored energy due to isotropic hardening, where κ is the isotropic hardening variable (i.e., accumulated plastic strain). The Helmholtz free energy function used for the bound elastomer can be written as

$$W_{b-elas} = \frac{\mu}{2}(I_1 - 3) - \mu \ln(J) + \frac{K}{4}(J^2 - 1 - 2 \ln(J)) \quad (5)$$

$$W_{b-isot} = Q \left(\kappa + \frac{e^{-\beta\kappa}}{\beta} \right) \quad (6)$$

It should be noted that the inclusion of isotropic hardening in the model results in the dependence of the yield stress on the accumulated plastic strain, i.e., $\sigma_y = \sigma_y(\kappa)$. This incorporates the behavior of the bound rubber depending on loading history and accounts for yielding of the glassy bridges. The final form of the constitutive equations is summarized in Table 1.

Table 1. Constitutive Equation for Finite Plasticity with Isotropic Hardening

stress tensors	$S = 2F_p^{-1} \frac{\partial W_{b-elas}}{\partial C_e} F_p^{-T}, Y = CS$
evolution equations	$\dot{C}_p = 2\dot{\Lambda} \frac{Y^D C_p}{\sqrt{Y^D(Y^D)^T}}, \dot{\kappa} = \sqrt{\frac{2}{3}} \dot{\Lambda}$
yield function	$\Phi = \sqrt{Y^D(Y^D)^T} - \sqrt{\frac{2}{3}} (\sigma_y - R), R = -Q(1 - e^{-\beta\kappa})$
Kuhn–Tucker conditions	$\dot{\Lambda} \geq 0, \Phi \leq 0, \dot{\Lambda}\Phi = 0$

S is the second Piola–Kirchoff stress tensor and Y another stress-like quantity. $\dot{\Lambda}$ denotes the plastic multiplier and $(\cdot)^D$ the deviatoric part of the tensor. Q and β are isotropic hardening parameters. The set of material parameters is completed by the yield stress σ_y .

Modeling of Bound Rubber and Its Glass–Rubber Transition. The formation of bound rubber is accounted for by a shift of glass transition temperature of elastomer in the

vicinity of a filler particle as described by Merabia et al.²⁴ This is represented using the following equation:

$$\theta_g(z) \approx \theta_{g0} \left(1 + \left(\frac{\delta}{z} \right)^{1/\nu} \right) \quad (7)$$

Here θ_{g0} is the bulk glass transition temperature, z is the distance from the particle, δ a length value which depends on matrix–filler interaction and ν is the exponent for correlation length in 3d percolation. The change in glass transition temperature as a function of distance and interaction length value is plotted in Figure 5.

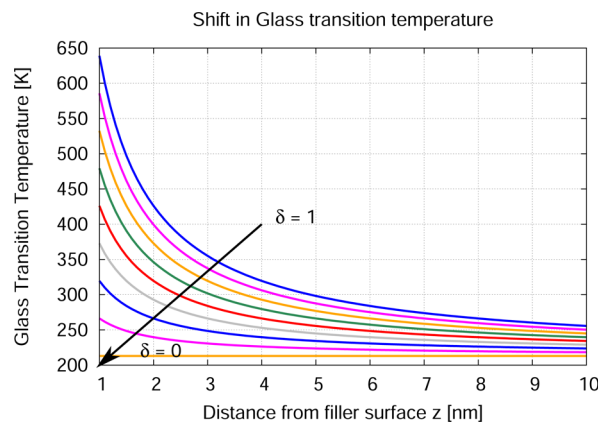


Figure 5. Local glass transition temperature $\theta_g(z)$ as a function of distance z from the filler surface for different matrix–filler interactions δ .

As mentioned earlier, in a system of filled elastomers the matrix is divided into two phases namely bound and the bulk region. The behavior of the bound region transforms from the glassy state close to the filler surface to the rubbery state away from the filler surface. Under a given loading condition the distance z of the material point surrounding the filler particle can change resulting in a change of the glass transition temperature. This in turn will vary the thickness of the bound rubber. This implies that the bound region does not have a discrete boundary. Hence, to incorporate the transition of bound rubber from glassy phase to the rubbery phase i.e. bulk elastomer, the strain energy density function used to represent the matrix (both bulk and bound rubber) is additively decomposed into W_b for bound elastomer and W_r for bulk elastomer as shown in eq 4. The factor ϕ is represented by an exponential function as shown below:

$$\phi = \frac{1}{1 + e^{2w\Delta\theta}} \quad (8)$$

The difference $\Delta\theta = \theta - \theta_g(z)$ is the difference between local temperature and the local glass transition temperature which decreases with the increase in distance from the filler surface. w is a fitting parameter to replicate the slope of the transition phase. From Figure 6, it is clear that the limit of the bound region thickness is within the transition region.

For different values of ϕ eq 4 can be rewritten as

$$\begin{aligned} \phi = 1 &\rightarrow W_{matrix} = W_b \\ \phi = 0 &\rightarrow W_{matrix} = W_r \\ 0 < \phi < 1 &\rightarrow W_{matrix} = \phi W_b + (1 - \phi) W_r \end{aligned} \quad (9)$$

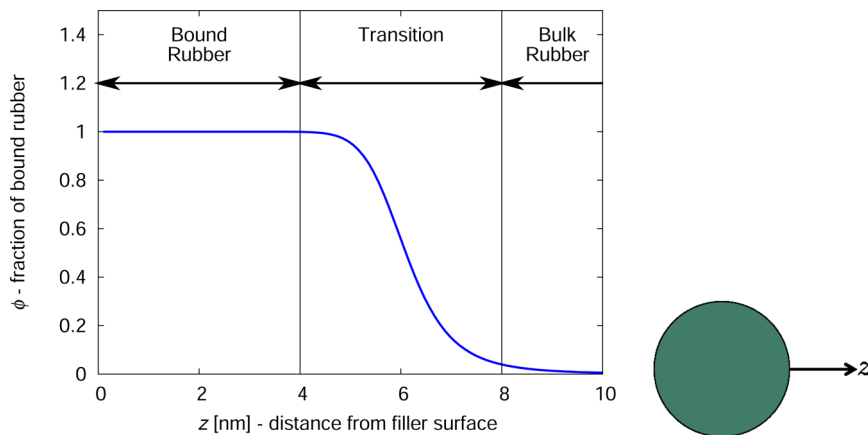


Figure 6. Transition of the strain energy function with respect to the distance from filler surface.

Using the rule of mixture formulation (eq 9), the stiffness of the matrix material can vary from a very stiff glassy like polymer, i.e., bound rubber ($\phi = 1$, close to the filler surface) to rubbery matrix ($\phi = 0$, away from the filler surface). The matrix is a mixture of bound rubber and rubbery matrix when $0 < \phi < 1$. As mentioned in the previous section, bound region is modeled using the concept of finite plasticity. This is used to account for the yielding and healing of the bound rubber. Such a formulation allows for the properties of the matrix close to the filler surface to be stiffer or softer under different loading conditions.

5. MICROMECHANICAL MODELING OF FILLED ELASTOMER

The modeling methodology adopted in this work assumes that the continuum mechanics framework holds down to the length scale of carbon black particles. This is a practical compromise between significant computational cost and morphological complexity to be captured. In particular, a micro-nano scale level is selected to capture the representative morphology of the nanocomposite using the concept of representative volume elements (RVE). At this level the carbon black aggregates and polymer matrix are each modeled as continua. Each RVE is composed of two components: (i) carbon black particles and (ii) elastomer matrix. As already mentioned the matrix is further divided into the two phases (i) bound elastomer which is in its glassy state and (ii) bulk elastomer which is in its rubbery phase. In the present approach, it is assumed that each point of a macroscopic continuum is associated with an RVE, characterizing the local microstructure. However, here we concentrate on uniform macroscopic deformations; hence, the behavior predicted from a single RVE allows us to determine the macroscopic response of the whole nanocomposite. The entire methodology is summarized in Figure 7.

In this work, we consider an ideal case of randomly distributed particles without overlaps and formation of aggregates. 3d stochastic distributions of spherical filler particles within representative volume elements are generated using a random generation algorithm restricting the radius of the circles to r_p and the number of spheres by the volume fraction. A simple standard uniform distribution algorithm is used to generate a random point within an RVE. Single spheres each representing a single particle are then placed on the generated point. After the particle is placed in its position, a check is implemented to find out whether the recently placed particle

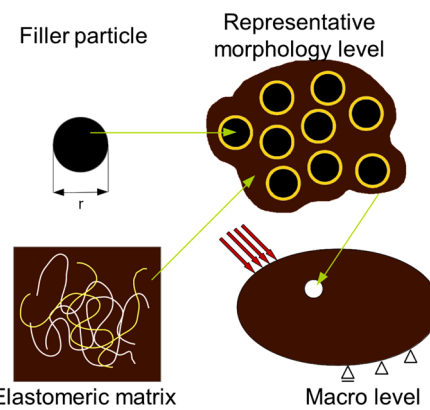


Figure 7. Modeling methodology used.

intersects with any of the already existing particles. In case of intersection, the particle is rejected, and the next trial particle is tested against the intersection criterion. This loop is carried out until the last particle is allocated a place within the RVE. A noteworthy feature, clearly visible in Figure 8, is the tendency

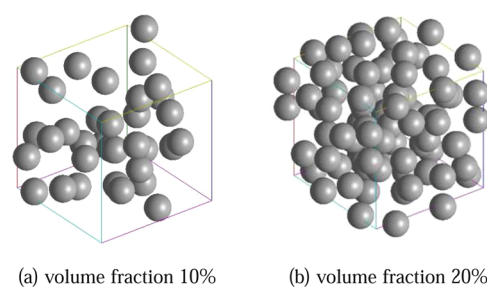


Figure 8. Representative volume elements of for different filler volume fractions.

for particles to be grouped into clusters, when required to fit into an RVE at a particular volume fraction, even though they were placed in position with random location and random orientation, subject only to the nonoverlapping criterion. This suggests that there exists a volume fraction above which the orientation of neighboring particles becomes correlated—particles grouping together into larger clumps of effective particles. Examples for RVEs with different volume fractions are shown in Figure 8.

The particle-placing algorithm is combined with a part generation tools to create the geometry of the internal structure. The generated geometry is then exported to meshing tool where the finite element models of filled elastomers at the RVE level is generated. An example of a typical mesh is shown in Figure 9. This mesh contains approximately 983400



Figure 9. Mesh of a sample RVE.

tetrahedral elements. Linear tetrahedral elements are used to model the filler particles and bound elastomer region whereas hybrid tetrahedral element have been used to model the bulk elastomer region. The bound region has been meshed fine enough to adequately capture its nonlinear effects. One must note that with increase of filler volume fraction the complexity of the internal structure increases. To achieve a good mesh quality for such systems with complex internal structure is challenging.

6. NUMERICAL SIMULATIONS

In this section, example numerical simulations are presented illustrating the explained modeling concept discussed in the previous sections. These examples serve to validate the presented modeling concept.

Using the rule of mixtures, the transition between bound and bulk rubber can be realistically displayed. For the bulk rubber, the Arruda-Boyce model (see section 2) is used whereas the bound rubber is represented by the elasto-plastic model explained in section 4. Thereby, the bound rubber is much stiffer than the bulk rubber. An advantage of working with the mixture theory is the fact that the material parameters for the two phases can be chosen independently of each other. Since the system is modeled using the rule of mixtures the material parameter for the individual components of the system can be chosen independently. For the soft bulk material which is rubbery in nature the material parameters have been obtained by fitting the Arruda-Boyce model to the experimental data provided by Treloar²⁹ for vulcanized rubber. Bound rubber is considered to be glassy and hence rather stiff. Due to the lack of suitable experimental data for the glassy rubber the material parameters for the bound rubber are assumed such that it represents the mechanical behavior of a stiff elastomer under deformation. Both the bulk and bound phases of the matrix are considered to be incompressible. The material parameters are given in Table 2. The carbon black particles are considered to

Table 2. Material Parameters

bulk rubber		bound rubber	
variable	value	variable	value
n	$8.05 \times 10^{17} \text{ mm}^{-3}$	μ	3355 N/mm^2
k	$1.3806488 \times 10^{-23} \text{ J K}^{-1}$	K	164430 N/mm^2
θ	300 K	σ_y	100 N/mm^2
N_0	5	Q	100 N/mm^2
K	168 N/mm^2	β	1.5

be isotropic and linear elastic, and hence are described in terms of two elastic constants: (a) the Young modulus, $E_{cb} = 200 \text{ GPa}$ and (b) the Poisson ratio, $\nu = 0.2$. The generated examples are subjected to cyclically increasing uniaxial tension with symmetric boundary conditions.

Example 1. The simulation results for loading of the sample with an volume fraction of 20% is shown in Figure 10. From the

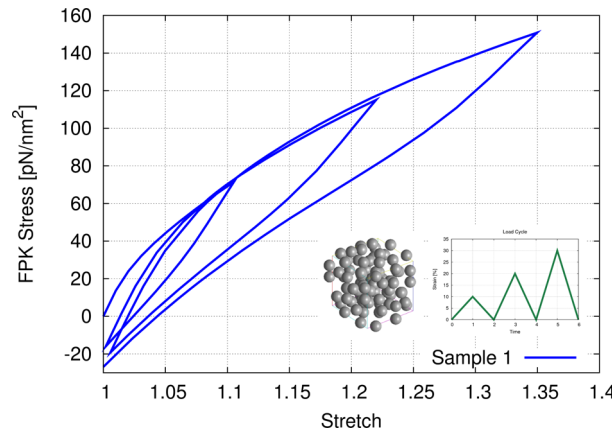


Figure 10. Stress-strain curve for loading of numerical example in X direction.

graph we can observe a hysteresis in the stress-strain curve for the given loading cycle. The hysteresis can be attributed to the yielding of glassy bridges which results in a permanent set in the system. We observe that the permanent set increases with increase in loading amplitude suggesting that the number of glassy bridges yielding increases as the loading amplitude increases. The curve obtained can also be considered to be qualitatively similar to the Mullins effect as shown in Figure 11. It is also observed that on reloading the samples the stress-strain curve follows a stiffer path.

While setting up the internal structure of the system it cannot be avoided that the distribution of the fillers in the RVE is not perfectly isotropic, see Figure 9. Hence, loading the sample in different directions yields different results. Figure 12 shows how different microstructures with the same volume fraction influences the stress-strain behavior.

We can observe a difference in the obtained stress-strain curves, suggesting that anisotropy in the system is induced due to the difference in the internal structure. This also leads to the formation of different filler networks in the loading and in the opposite direction, resulting in different numbers of glassy bridges that yield under the given loading cycle. This results in a qualitatively similar behavior but of a different magnitude. In fact, the induced anisotropy visible in the Mullins type material behavior can also be attributed to that.

The contour plots for internal strains are as shown in Figure 13. From the plots, we can observe the local strain amplification

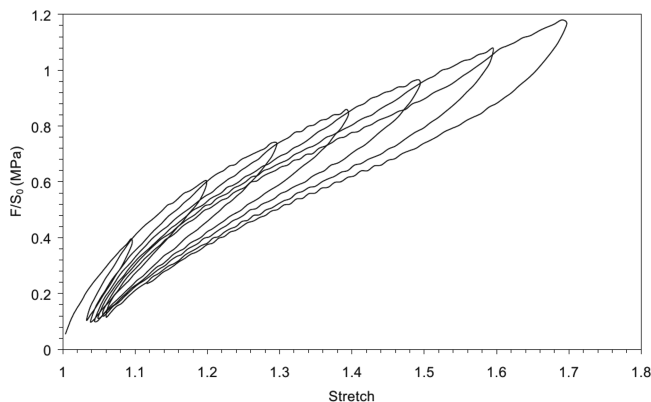


Figure 11. Mullins' effect at small and moderate deformation observed on a 50 phr carbon-black filled SBR submitted to cyclic uniaxial tension.¹⁷

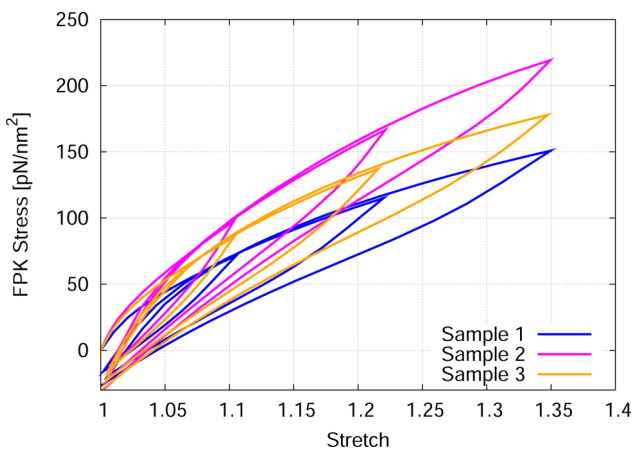


Figure 12. Comparison of loading on numerical example in X and Y direction.

in the bulk part of the matrix between two filler particles which are close to each other. This can be explained as follows. Due to the closeness of the two particles, a small number of elastomer chains occupy the space between these particles. Under loading, filler particles undergo nonaffine movement within the matrix, which results in extensive stretching of the elastomer chains between these filler particles when compared to the bulk of the matrix. This results in a local strain amplification.

Example 2. Now comparing the simulation results for different volume fraction (Figure 14), we observe that the hysteresis loop obtained for sparsely filled system is less pronounced than for highly filled samples, which is in concurrence with the results reported in literature. Such a difference can be explained by the absence of the filler network in loading direction, which in turn results in a small number of glassy bridges that yield during the given loading cycle.

7. CONCLUSION AND OUTLOOK

The system of filled elastomer has been successfully modeled at a microscopic level using the finite element method. Different phases of the microstructure are explicitly resolved in the full field simulation. The transition of material properties from stiff to rubbery phase in the bound region has also been modeled, using the theory of shift in glass transition temperature in the vicinity of the filler particle. The results obtained from the simulation, using micromechanically motivated material models for the bulk and bound elastomer region along with a physically motivated finite plasticity model (i.e. considering only plastic flow dissipation mechanism) is in good qualitative agreement with the experimental results. Even though the reformation of the glassy bridges has not been the main focus of this work, the model is capable of theoretically showing the Mullins effect. From the simulated examples it can be concluded that the effect of morphology of the microstructure strongly depends on the filler volume fraction, which in turn increases or decreases the number of load carrying glassy bridges in the system. Therefore, it can be concluded that increase or decrease in stiffness of filled elastomer is directly related to the number of glassy bridges in

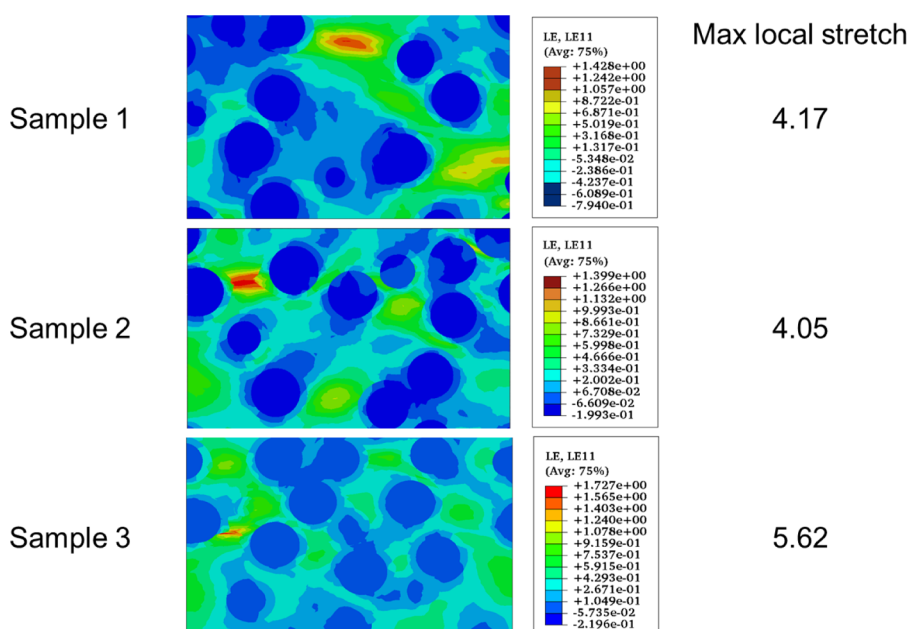


Figure 13. Strain contour plots showing local strain amplification for a global displacement for 30% strain.

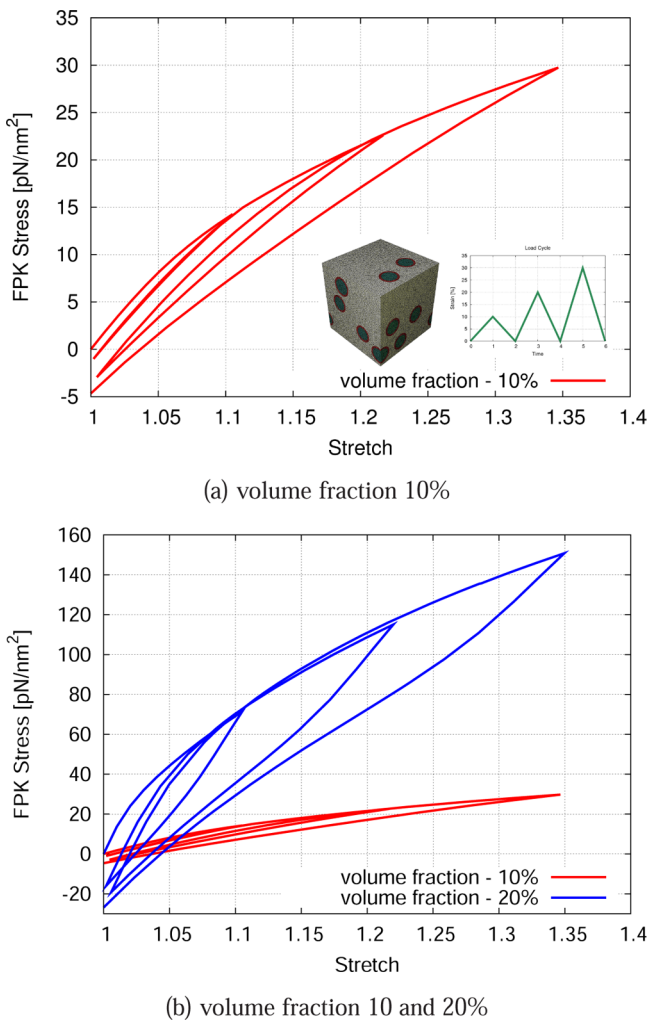


Figure 14. Comparison of the stress-strain curve obtained for different volume fractions.

the system and its morphology under loading. As this is part of an ongoing work, this model will be extended to incorporate the effects of microstructure morphology on viscous behavior of filled elastomers and to simulate the Payne effect. The advantage of using such a full field simulation to model particle-reinforced elastomers is that the effect of different microstructural behavior on the mechanical properties of the system can be explicitly investigated.

APPENDIX 1: BASIC CONTINUUM QUANTITIES

In this section, the continuum quantities used in this paper have been elaborated:

- 1 Deformation gradient is a tensorial quantity which describes the mapping of a material line element dX in the initial (undeformed) configuration B to a line element dx in the current (deformed) configuration $\varphi(B)$ as (see Figure 15):

$$dx = F dX; \quad F = \frac{\partial x}{\partial X}$$

- 2 J is the determinant of the deformation gradient. It also depicts the transformation between the initial infinitesimal volume element (dV) and the corresponding infinitesimal current volume element (dv): $dv = J dV$.

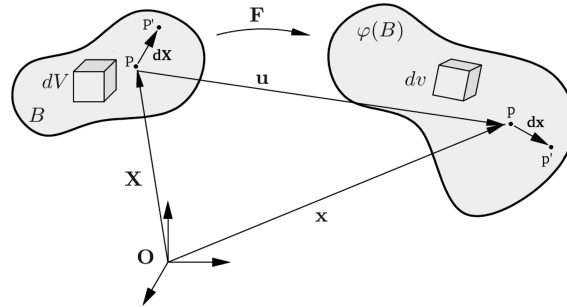


Figure 15. Deformation of the body B .

- 3 As elastomers are capable of undergoing large deformations, finite (large) strain theory is considered in which rotations and strains can be arbitrarily large. $C = F^T F$ is the right Cauchy–Green tensor. It is part of the relation $dx^T dx = dX^T F^T F dX = dX^T C dX$.
- 4 I_1 , I_2 and I_3 are the invariants of C which are often used in the expressions for strain energy density functions W . The first invariant is defined as $I_1 = \text{tr}(C)$.
- 5 To describe finite strains, one frequently uses the Green–Lagrange strain tensor $E = ((1/2)(C - I))$, which represents a physically based strain measure valid for arbitrarily large strains and rotations.
- 6 Among many possible stress measures, the crucial quantities are the “true” stress and the “engineering” stress. The former refers a force to the deformed cross-section while the second refers a force to the undeformed cross-section. The corresponding tensorial quantities are σ (true/Cauchy stress tensor) and P (engineering/first Piola–Kirchhoff stress tensor). It is often advisable to work with $S = \partial W / \partial E$, because S is symmetric in contrast to P . S and P are related by $P = FS$. However, S does not have a physical meaning of its own.

APPENDIX 2: KUHN–TUCKER CONDITIONS

In this section, Kuhn–Tucker conditions have been elaborated. The Kuhn–Tucker conditions are necessary to obtain an optimal solution in nonlinear modeling. In this case, it helps to differentiate between elastic and plastic loading/unloading scenarios. The Kuhn–Tucker conditions are as follows:

$$\dot{\Lambda} \geq 0, \quad \Phi \leq 0, \quad \dot{\Lambda}\Phi = 0$$

Here, $\dot{\Lambda}$ is the plastic multiplier and Φ is the yield function. These conditions evaluate the following scenarios:

$\Phi > 0 \rightarrow \dot{\Lambda} = 0$ material is under elastic loading and there is no plastic deformation

$\Phi = 0$ and $\dot{\Lambda} = 0$ material has yielded but there is no plastic deformation on further loading

$\Phi = 0$ and $\dot{\Lambda} > 0$ material has yielded and deforms plastically on further loading

AUTHOR INFORMATION

Corresponding Author

*(D.S.) E-mail: deepanshu.sodhani@rwth-aachen.de.

Notes

The authors declare no competing financial interest.

ACKNOWLEDGMENTS

We would like to sincerely thank the DFG (Priority Program SPP1369 “Interphases and Interfaces”) for the funding and

Deutsches Institut für Kautschuktechnologie e.V. (DIK) for their support. We would also like to thank our Dr. Ivaylo Vladimirov for his gracious support in the continuum mechanical material model.

■ REFERENCES

- (1) Payne, A. R.; Kraus, G. *Reinforcement of elastomers*; Interscience: New York, 1965; p 69.
- (2) Mullins, L. *Rubber Chem. Technol.* **1969**, *42*, 339–362.
- (3) Huber, G.; Vilgis, T. A. *Kautschuk Gummi Kunstst.* **1999**, *52*, 102–107.
- (4) Berriot, J.; Montes, H.; Lequeux, F.; Long, D.; Sotta, P. *Macromolecules* **2002**, *35*, 9756–9762.
- (5) Klüppel, M. *Chem. Mater. Sci.* **2003**, *164*, 1–86.
- (6) Vilgis, T.; Heinrich, G.; Klüppel, M. *Reinforcement of Polymer Nano-Composites: Theory, Experiments and Applications*; Cambridge University Press: London, 2009; p 209.
- (7) Schröder, A.; Klüppel, M.; Schuster, R. H. *Macromol. Mater. Eng.* **2007**, *292*, 885–916.
- (8) Dupres, S.; Long, D. R.; a. Albouy, P.; Sotta, P. *Macromolecules* **2009**, *42*, 2634–2644.
- (9) Schmoller, K. M.; Bausch, A. R. *Nat. Mater.* **2013**, *12*, 278–281.
- (10) Govindjee, S.; Simo, J. *J. Mech. Phys. Solids* **1991**, *39*, 87–112.
- (11) Marckmann, G.; Verron, E.; Gornet, L.; Chagnon, G.; Charrier, P.; Fort, P. *J. Mech. Phys. Solids* **2002**, *50*, 2011–2028.
- (12) Arruda, E. M.; Boyce, M. C. *J. Mech. Phys. Solids* **1993**, *41*, 389–412.
- (13) Göktepe, S.; Miehe, C. *J. Mech. Phys. Solids* **2005**, *53*, 2259–2283.
- (14) Lin, C.-R.; Lee, Y.-D. *Macromol. Theory Simul.* **1996**, *5*, 1075–1104.
- (15) Dargazany, R.; Itskov, L. *PAMM* **2009**, *9*, 349–350.
- (16) Lorenz, H.; Freund, M.; Juhre, D.; Ihlemann, J.; Klüppel, M. *Macromol. Theory Simul.* **2011**, *20*, 110–123.
- (17) Diani, J.; Fayolle, B.; Gilormini, P. *Eur. Polym. J.* **2009**, *45*, 601–612.
- (18) Lorenz, H.; Klüppel, M.; Heinrich, G. *ZAMM—J. Appl. Math. Mech./Z. Angew. Math. Mech.* **2012**, *92*, 608–631.
- (19) Gusev, A. A. *Macromolecules* **2006**, *39*, 5960–5962.
- (20) Gusev, A. A.; Lurie, S. A. *Macromolecules* **2009**, *42*, 5372–5377.
- (21) Leblanc, J. L. *J. Appl. Polym. Sci.* **2000**, *78*, 1541–1550.
- (22) Edwards, S. F.; Vilgis, T. A. *Rep. Prog. Phys.* **1988**, *51*, 243.
- (23) Böhl, M.; Reese, S. *Int. J. Solids Struct.* **2006**, *43*, 2–26.
- (24) Merabia, S.; Sotta, P.; Long, D. *Macromolecules* **2008**, *41*, 8252–8266.
- (25) Reese, S.; Wriggers, P. *Comput. Methods Appl. Mech. Eng.* **1997**, *148*, 279–298.
- (26) Dettmer, W.; Reese, S. *Comput. Methods Appl. M. Eng.* **2004**, *193*, 87–116.
- (27) Vladimirov, I. N.; Pietryga, M. P.; Reese, S. *Int. J. Numerical Methods Eng.* **2008**, *75*, 1–28.
- (28) Vladimirov, I.; Pietryga, M.; Reese, S. *J. Mater. Process. Technol.* **2009**, *209*, 4062–4075.
- (29) Treloar, L. *Trans. Faraday Soc.* **1944**, *40*, 59–70.